HCCI 조건에서의 희박 정상-헵탄/공기 혼합물의 점화에 관한 직접 수치 모사

유춘상*† · Jackquiline H. Chen**

DNS of ignition of a lean *n*-heptane/air mixture under HCCI conditions

Chun Sang Yoo*†, Jackquiline H. Chen**

ABSTRACT

The effect of thermal stratification on the ignition of a lean homogeneous *n*-heptane/air mixture at constant volume and high pressure is investigated by direct numerical simulations (DNS) with a new 58-species reduced kinetic mechanism. 2-D DNS are performed in a fixed volume with a two-dimensional isotropic velocity spectrum and temperature fluctuations superimposed on the initial scalar fields. The influence of variations in the initial temperature field, imposed by changing the mean and variance of temperature on multi-stage ignition of a lean n-heptane/air mixture is studied. In general, the mean heat release rate increases more slowly with increasing thermal stratification regardless of the mean initial temperature. Ignition delay decreases with increasing thermal stratification for high mean initial temperature relative to the negative temperature coefficient (NTC) regime. It is, however, retarded with increasing thermal fluctuations for relatively low mean initial temperature resulting from a longer overall ignition delay of the mixture. Displacement speed and Damköhler number analyses reveal that the high degree of thermal stratification induces deflagration rather than spontaneous ignition at the reaction fronts, and hence, the mean heat release rate is smoother subsequent to thermal runaway occurring at the highest temperature regions in the domain. These results suggest that the critical degree of thermal stratification for smooth operation of homogeneous charge compression-ignition (HCCI) engines depends on both the mean and fluctuations in initial temperature which should be considered in controlling ignition timing and preventing an overly rapid increase in pressure in HCCI combustion.

Key Words : DNS, *n*-heptane reduced mechanism, thermal stratification, auto-ignition

1. Introduction

Homogeneous charge compression-ignition (HCCI) combustion prototype engines are being developed as an alternative to conventional gasoline spark-ignition (SI) and diesel compression ignition (CI) engines. HCCI combustion under lean, dilute, high-pressure and low-temperature conditions has the potential to provide high diesel-like efficiency with very low nitrogen oxides (NO_x) and particulate emissions. At these conditions HCCI combustion is thought to occur primarily through volumetric auto-ignition, largely in the absence of flames, and hence is primarily controlled by chemical kinetics of the fuel-air mixture. Hence, one of the key issues in the development of HCCI engines is how to control the ignition timing and the rate of

* 유니스트 기계신소재공학부
** Combustion Research Facility, Sandia National Labs
† 연락저자, csyoo@unist.ac.kr

pressure rise or heat release rate under a wide range of load conditions [1. 2]. In particular, an excessive rate of pressure rise under high-load condition can result in engine knock, reducing the engine integrity and hence, must be avoided through careful engine design and operation.

Over the past decade, numerous experimental and numerical studies on HCCI combustion have been conducted. The influence of thermal stratification and equivalence ratio fluctuations on the characteristics of HCCI combustion has been extensively investigated by the engine research community [1-12]. In these studies, thermal stratification was proposed as a means to spread out the rate of pressure rise under high-load conditions [1, 3, 4, 6-8]. In the presence of large temperature fluctuations, auto-ignition first occurs in hotter mixtures and then spreads to the remaining charge sequentially, such that combustion does not occur simultaneously throughout the engine cylinder.

On the other hand, mixture inhomogeneity was proposed to enhance and stabilize the HCCI combustion under low-load conditions [9-12]. Enhanced combustion could be achieved for a low mean equivalence ratio if locally rich pockets are present, which burn hotter and provide heat and radicals to adjacent leaner mixtures, and hence, significantly increase combustion efficiency. In addition to the mixture inhomogeneity, delayed-fuel injection was also considered to further increase temperature and composition stratification from the mixing process [9]. Recently, spark-assisted HCCI combustion [13, 14] was also proposed to improve combustion efficiency in low-load engine operation and to control ignition timing. In spark-assisted HCCI combustion, a spark-ignited flame ultimately leads to compression heating and subsequent auto-ignition of the leaner mixtures, and hence both flame and auto-ignition can coexist during the engine operation.

Ignition characteristics of HCCI combustion were also elucidated by direct numerical simulations (DNS) with detailed chemical kinetics. Two-dimensional DNS of ignition of lean hydrogen/air mixtures with temperature inhomogeneities [15-17] revealed that, for sufficiently large temperature fluctuations, deflagrations occur rather than volumetric auto-ignition, and consequently, the rate of heat release is spread out as the deflagrations propagate through the mixture. The transition between the normal deflagration regime and the subsonic spontaneous ignition front propagation regime was identified originally by Zel'dovich [18], although one significant difference between his original theory and the DNS findings is that it is the instantaneous, rather than initial thermal gradient, that is the relevant criteria in distinguishing between combustion regimes.

In addition, the effect of flow strain on the transient auto-ignition of mixtures has been studied in various configurations. Liu et al. [19, 20] investigated the auto-ignition of diluted *n*-heptane jet flowing against heated air at high pressures in a one-dimensional counterflow configuration with steady and unsteady impulsive strain rate. More recently, Bansal et al. [21] studied the response of auto-ignition of one-dimensional nonpremixed *n*-heptane/air counterflow subjected to harmonic flow oscillations. From two-dimensional DNS, Im et al. [22] studied the ignition of a hydrogen/air scalar mixing layer in a homogeneous turbulence, and Echekki and Chen [23] investigated auto-ignition of non-homogeneous hydrogen/air mixtures prescribed by a scalar spectrum in homogeneous turbulence. These studies show that strong turbulence leads to intense mixing rates or high strain rate inhibits ignition by dissipating heat and intermediate species from ignition kernels.

Experimental studies, however, can still provide limited information including overall pressure rise, concentrations of NO_x, CO, and unburnt hydrocarbon emissions, and 2-D line-of-sight chemiluminescence or planar images of select species. Detailed characterization of chemical reactions occurring inside an engine chamber is still elusive. Similarly, previous multi-dimensional DNS were performed only with the simplest chemistry, hydrogen-air, owing to the prohibitive computational cost. As such, the results of the DNS were not directly applicable to the design and operation of practical

Table 1 Numerical and physical parameters of the DNS for different mean and RMS of initial temperature

Case	T_0 (K)	T' (K)	l_e (mm)	u'(m/s)	τ_t (ms)	τ_{ig}^0 (ms)	L (mm)	N
1	850	7.5	1.24	0.5	2.49	2.49	3.2	640
2	850	15	1.24	0.5	2.49	2.49	3.2	640
3	850	30	1.24	0.5	2.49	2.49	3.2	640
4	850	60	1.24	0.5	2.49	2.49	3.2	1280
5	850	100	1.24	0.5	2.49	2.49	3.2	1280
6	934	15	1.24	0.5	2.49	2.49	3.2	640
7	934	30	1.24	0.5	2.49	2.49	3.2	640
8	934	60	1.24	0.5	2.49	2.49	3.2	640
9	934	100	1.24	0.5	2.49	2.49	3.2	1280
10	1008	15	1.24	0.5	2.49	2.49	3.2	640
11	1008	30	1.24	0.5	2.49	2.49	3.2	640
12	1008	60	1.24	0.5	2.49	2.49	3.2	1280

hydrocarbon-fueled engines, although fundamentals of hydrogen/air ignition at constant volume under HCCI conditions were elucidated.

Therefore, the objective of the present study is two-fold: (i) to understand the ignition characteristics of practical hydrocarbon/air mixtures under HCCI conditions, and (ii) to provide strategies to control the rate of heat release in HCCI combustion by performing two-dimensional parametric DNS, systematically varying the initial mean and variance of the temperature. In this study *n*-heptane is adopted as a surrogate fuel for large hydrocarbon fuels which generally exhibit two-stage ignition under HCCI conditions. Note that *n*-heptane has been widely used as a primary reference fuel (PRF) to investigate the characteristics of HCCI combustion in many previous studies [24-28].

2. Numerical methods and initial conditions

The compressible Navier-Stokes, species continuity, and total energy equations were solved using the Sandia DNS code, S3D [29]. A fourth-order explicit Runge-Kutta method by Kennedy and Carpenter [30] was used for time integration. The solution was spatially discretized using an eighth-order central differencing scheme. A tenth-order filter was employed to remove any spurious high-frequency fluctuations in the solution [31]. CHEMKIN and TRANSPORT software libraries [31, 32] were linked with S3D to evaluate reaction rates and thermodynamic and mixture-averaged transport properties. Periodic boundary conditions were imposed in all directions such that ignition of a *n*-heptane/air mixture occurs at constant volume.

The initial uniform equivalence ratio, ϕ, and pressure, p_0, are 0.3 and 40 atm, respectively. Note that $\phi = 0.3$ is adopted to elucidate the ignition characteristics of a *n*-heptane/air mixture under high load conditions [1, 3]. Several parametric studies were performed to understand the effects of varying the initial mean and fluctuation of temperature and of varying the ratio of turbulence to ignition delay timescale. A total of twelve different DNS cases were performed in the parameter space of initial physical conditions: mean temperature T_0; temperature fluctuation root mean square (RMS) T'; most energetic turbulent length scale l_e; turbulence

velocity fluctuation u'; turbulence time-scale τ_t; and homogeneous ignition delay τ_{ig}^0. Henceforth, τ_{ig} represents the time at which the maximum mean heat release rate occurs, and the superscript 0 corresponds to the zero-dimensional simulation at constant volume. Details of the physical and numerical parameters for the first twelve cases are presented in Table 1.

Note that in real HCCI engines, ignition delay is approximately 2 ms and turbulence time-scale is ~ $O(1\,\mathrm{ms})$ [5, 16, 17]. The parameters in the present study were selected so that the turbulence time-scale, $\tau_t = l_e/u'$, is comparable to the homogeneous ignition delay of the mixture at the same initial mean temperature and pressure, τ_{ig}^0, which significantly enhances turbulence-chemistry interaction. Also note that temperature fluctuations prior to the ignition in HCCI engines are approximately 15~ 20 K [9], which are much less than T' = 60 or 100 K for the present study. However, these high temperature fluctuations can be achieved through direct injection or delayed-fuel injection in HCCI combustion such that it is also important to understand the ignition characteristics of HCCI combustion with high T'.

The computational domain is a two-dimensional square box with each size of the domain, L, of 3.2 mm, discretized with N = 640 grid points for most cases. The corresponding grid resolution is 5.0 μm. This fine grid resolution is needed to resolve the ignition structure at high pressure. For several of the cases with large T' (i.e., Cases 4, 5, 9, and 12), 2.5 μm grid resolution is required to resolve thin flame-like structures. The most energetic length scale of the temperature fluctuation, l_{Te}, is 1.0 mm for all cases. Typical profiles of initial temperature and vorticity in the DNS are shown in Fig. 1.

While the integral scale of the temperature fluctuation in the DNS is typically smaller than in a real engine, the length scale of the fluctuation does not control the evolution of the temperature gradient or its dissipation rate which controls the mode of combustion. Assuming equilibrium between production and dissipation of thermal fluctuations, the thermal dissipation rate is proportional to the ratio of the temperature RMS to the turbulence time-scale [33]. Hence, although the DNS integral length scales are smaller than those in an engine, as long as the turbulence time-scale and temperature fluctuations are similar, the modes of combustion observed in the DNS will be relevant to modes in actual engines.

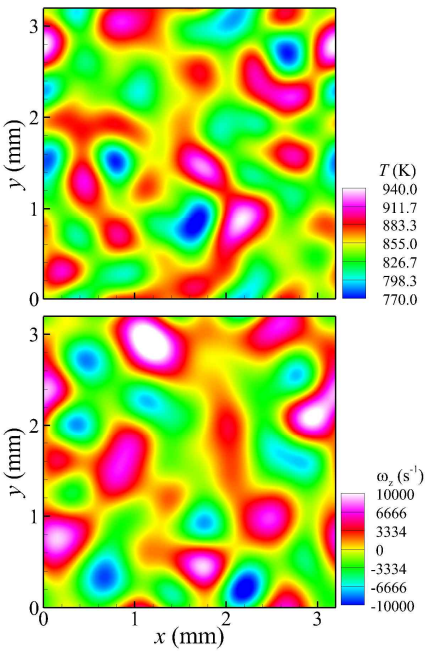

Figure 1. Initial profiles of temperature and vorticity for Case 3.

3. Effect of mean and RMS of initial temperature

In the first parametric study, the combined effect of mean and fluctuation of initial temperature on the ignition of a lean *n*-heptane/air mixture is investigated (see Table 1 for a description of detailed parameters). As discussed in Section 1, thermal stratification, achieved through either variations in mean or fluctuations in temperature, was proposed to prevent an excessive rate of pressure rise. Moreover, as the mean temperature of the engine chamber

prior to thermal runaway can significantly change the ignition delay, it is expected that the effect of T'' on the pressure rise can also be altered by the mean temperature of the fuel/air mixture. Therefore, three different initial mean temperatures near the negative temperature coefficient (NTC) regime were considered (i.e., T_0 = 850, 934, and 1008 K), all with identical homogeneous ignition delays (τ_{ig}^0 = 2.49 ms). The existence of the NTC regime is attributed to the transition of the ignition process from the low-temperature to intermediate-temperature chemistry.

In the NTC regime, the ignition process commences with the low-temperature chemistry, and then, heat release from the low-temperature chemistry triggers the intermediate-temperature chemistry, in which the low-temperature ignition process (e.g. thermal dissociation of heptylhydroperoxide, KET) ceases and H_2O_2 dissociation ($H_2O_2+M \rightarrow OH+OH+M$) determines the rate of chain branching. The H_2O_2 branching rates are initially lower than the KET branching rates prior to the transition, and thus, it leads to a two-stage ignition with the first stage ignition by the low-temperature chemistry and the second stage ignition by the intermediate-temperature chemistry [20].

Figure 2 shows τ_{ig}^0 as a function of initial temperature. The first-stage ignition delay, τ_{ig}^0, is also presented in the figure. While T_0 = 850 K and 934 K are within the NTC regime, T_0 = 1008 K is slightly outside of the NTC regime. Note also that two-stage ignition does not exist for $T_0 > 940$ K.

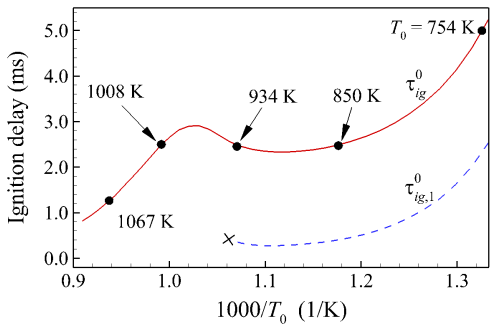

Figure 2. Homogeneous ignition delay at constant volume with initial pressure of 40 atm as a function of temperature

3.1 Overall combustion characteristics

For each mean initial temperature three to five DNS cases were performed with varying levels of temperature fluctuations, T''. Figure 3 shows the temporal evolution of mean heat release rate, $\bar{\dot{q}}$, for the cases. Three observations are noted from the figure. First, for the lower initial mean temperature cases with T_0 = 850 K (Cases 1-5), τ_{ig} is retarded with increasing T''; on the contrary, for the higher initial mean temperature cases with T_0 = 1008 K, τ_{ig} is reduced with increasing T'' (Cases 10-12). For T_0 = 934 K, τ_{ig} increases with small T'', but decreases with large T''. Therefore, the cases with T_0 = 934 K exhibit the combined effects of low and high mean temperatures near the NTC regime. Second, for all cases as T'' increases, $\bar{\dot{q}}$ is further spread out over time and the peak $\bar{\dot{q}}$ is reduced consistent with previous DNS of hydrogen/air ignition under HCCI conditions [17]. Third, the first-stage ignition delay for the cases with T_0 = 850 K is slightly decreased with T'' and the corresponding peak $\bar{\dot{q}}$ is also reduced. There is, however, no significant difference in the first-stage ignition delays for the cases with T_0 = 934 K. Note also that first-stage ignition is negligible for cases with T_0 = 1008 K.

The dependence of $\bar{\dot{q}}$ on T_0 and T'' is investigated by simply examining the initial temperature distributions of the DNS. The initial temperature distribution for each case spans a different range of ignition delays. Therefore, the overall ignition characteristics may be estimated from the initial distribution. Figure 4 shows the 95 % range of τ_{ig}^0 for initial mixtures with T'' = 60~K for T_0 = 850, 934 and 1008~K (i.e., Cases 4, 8, and 12, respectively). Note that small gaps between the lines in the figure are intentionally placed to clearly show the ranges. As shown in the figure, the range of τ_{ig}^0 for T_0 = 850, 934 and 1008 K are 2.33 - 7.18 ms, 1.57 - 2.90 ms, and 0.55 - 2.90 ms, respectively. Note that, for T_0 = 850 K (Case 4), the fastest ignition delay

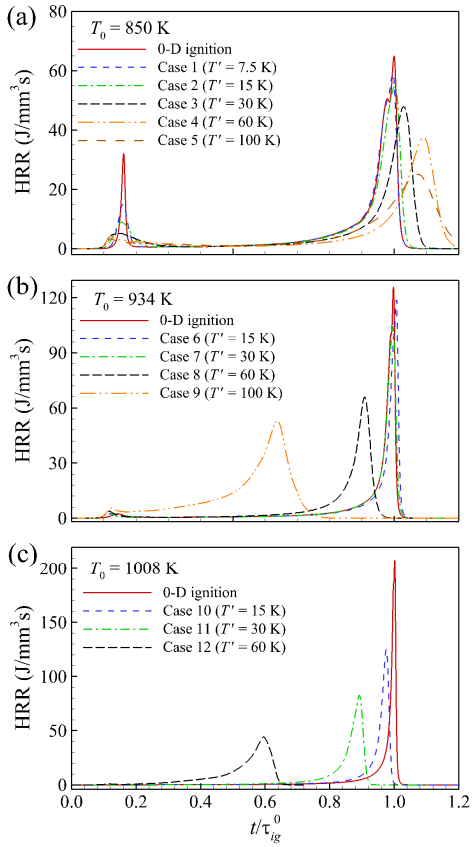

Figure 3. Temporal evolution of mean heat release rate with different temperature RMS for (a) T_0 = 850, (b) 934, and (c) 1008 K.

is comparable to the corresponding τ_{ig}^0 (= 2.49 ms) and the slowest ignition delay is three-times longer than τ_{ig}^0, much longer than the total time required for complete combustion (~ 3.0 ms, see Fig.3 (a)). Therefore, portions of the domain with long ignition delay significantly retard the overall combustion as shown in Fig. 3 (a).

On the contrary, for T_0 = 1008 K (Case 12), the fastest ignition delay is approximately five-times shorter than the corresponding τ_{ig}^0, such that the portions of the domain with short ignition delay accelerate the ignition progress over the homogeneous case, and hence, overall combustion occurs quickly. Note that, for T_0 = 934 K, T' = 100 K (Case 9) induces a similar degree of ignition enhancement as T' = 60 K (Case 12) with T_0 = 1008 K. Since T_0 = 934 K lies in the middle of the NTC regime, compared with T_0 = 1008 K cases, larger T' is required for the initial scalar field to include proportionately larger portions of the domain with higher initial temperature or shorter ignition delays. This simple estimate of the range of homogeneous ignition delays of mixtures shows that temperature fluctuations have a first-order effect on the ignition characteristics of *n*-heptane/air mixtures, with the sensitivities greatest away from the NTC regime.

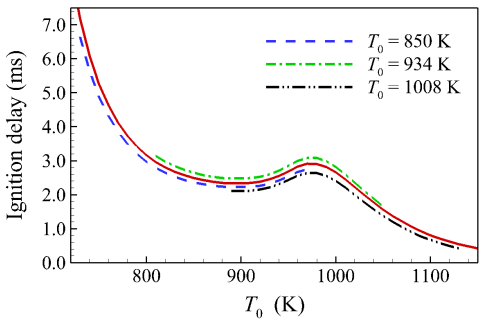

Figure 4. 95 % range of ignition delay with T' = 60 K for DNS with T_0 = 850, 934, and 1008 K at initial pressure of 40 atm

Hawkes et al.[17] found that deflagration due to large T' spreads out $\dot{\bar{q}}$ in the ignition of lean hydrogen/air mixtures. To verify this mechanism in the ignition of a *n*-heptane/air mixture, the overall structure of the heat release rate field is examined. Figure 5 shows isocontours of heat release rate, $\dot{q}$, for Cases 6-9 approximately at each τ_{ig}, normalized by the corresponding maximum heat release rate during the homogeneous ignition, $\dot{q}_m$= 125.8 J/mm^{3}s. It is readily observed from the figure that $\dot{q}$ occurs nearly simultaneously throughout the domain as spontaneous ignition for small T' (Case 6). However, high $\dot{q}$ occurs primarily at thin flame-like regions for large T' (Case 9), although relatively low $\dot{q}$ also occurs over a much broader area. Therefore, this suggests that the combustion mode is sensitive to variations with T'; i.e., the spontaneous ignition mode is predominant for small T' while the mixed mode of deflagration and spontaneous ignition occurs for large T'.

Similarly, for Cases 5 and 12 with large T', ignition is advanced due to the existence of locally hotter mixtures, and $\dot{\bar{q}}$ is spread out

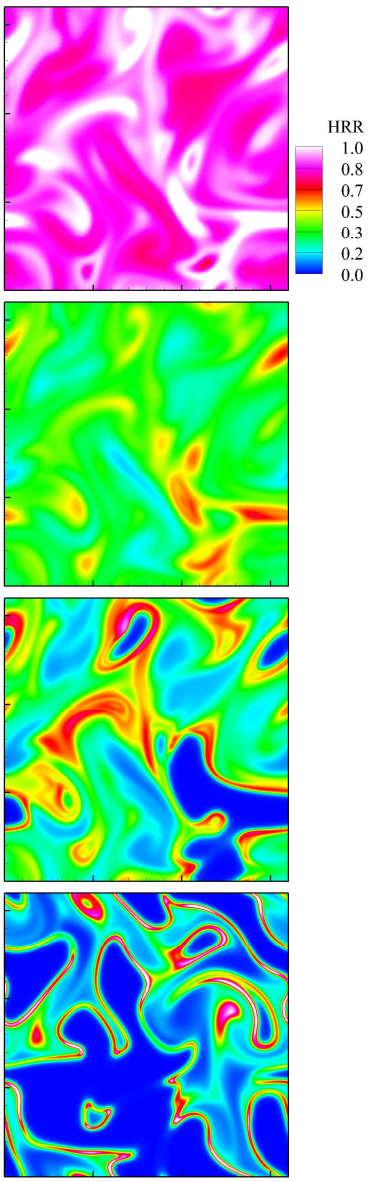

Figure 5. Isocontours of normalized heat release rate for Cases 6-9 (from top to bottom) at t/τ_{ig}^{0} = 1.0, 0.96, 0.88, and 0.60, respectively.

more as shown in Fig. 3 since a significant fraction of the mixture with long ignition delays are consumed by deflagrations. Thus overall, combustion is controlled by flame propagation characteristics. A detailed analysis pertaining to the propagation and chemical characteristics of deflagration and spontaneous

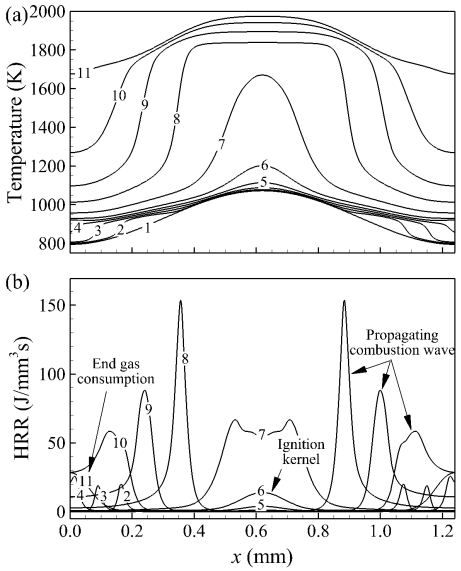

Figure 6. Temporal evolution of (a) temperature and (b) heat release rate with T_0 = 934 K and T' = 100 K. The equally spaced time sequence is numbered from 1 to 11, starting at 0.2 ms with an increment of 0.2 ms.

ignition modes is presented in the following sections.

3.2 Combustion modes - propagation speed and burning rate

In this section, the nature of the combustion modes for the cases with different T_0 and T' is elucidated using diagnostics previously developed in [16, 17]. Prior to examining the two-dimensional DNS cases, one-dimensional DNS reference cases are simulated using a sinusoidal temperature profile. The wavelength of 1.24 mm in the one-dimensional cases matches the most energetic length scale, l_e, in the 2-D DNS cases and the mean and RMS temperature, T_0 and T', also match the two-dimensional DNS cases. Figure 6 shows the temporal evolution of temperature and heat release rate profile for T_0 = 934 K and T' = 100 K corresponding to Case 9. Combustion progresses in the following manner: beyond the first-stage ignition (2-4 in Fig. 6), a high-temperature

ignition kernel develops in the middle of the domain (5-7 in Fig. 6) and subsequently propagating combustion waves emanate, traveling to the left and right of the domain (8-10 in Fig. 6); finally, the remaining gas is heated by compression and consumed as the propagating combustion wave approaches the boundary of the domain (11 in Fig. 6). Combustion progresses nearly the same as for ignition of a lean hydrogen/air mixture [16], except for the addition of first-stage ignition. Note also that the presence of a propagating front does not necessarily imply that the front is a deflagration wave. The nature of the propagating wave and the role of molecular diffusion need to be identified.

For this purpose, the density-weighted displacement speed, S_d^*, is adopted to distinguish between deflagrations and spontaneous ignition fronts [16, 17]; S_d^* is defined as:

$$S_d^* = \frac{1}{\rho_u |\nabla Y_k|}\left(\dot{\omega}_k - \frac{\partial}{\partial x_j}(\rho Y_k V_{j,k})\right), \qquad (1)$$

where Y_k, $V_{j,k}$, and $\dot{\omega}_k$ denote species mass fraction, species diffusion velocity in the j-direction and net production rate of species k, respectively, and ρ_u is the density of the unburnt mixture. ρ_u is calculated from the local enthalpy and fresh mixture condition assuming pressure and enthalpy remain constant across the front [16, 17]. In the present study, the isocontour of $Y_c = Y_{CO_2} + Y_{CO} = 0.04$ is chosen to evaluate the displacement speed. This particular isocontour coincides approximately with the location of maximum $\dot{q}$.

To understand the characteristics of propagating fronts in the simulations, it is necessary to compare S_d^* with the corresponding laminar flame speed, S_L. Note that unlike in the previous hydrogen/air DNS study [16], the laminar flame speed could not be obtained from a steady freely propagating flame computation using the PREMIX code [34] due to the highly reactive nature of the current n-heptane/air mixture. In this study, instead, the laminar flame speeds were estimated from transient 1-D reactive DNS. The DNS were initialized with a high-temperature ignition source such that a combustion wave emanates from the source, propagating into the reactive mixture ahead of it. Since auto-ignition in the reactive mixture does not occur prior to τ_{ig}^0, the speed of the propagating combustion wave, S_d^*, can be regarded approximately as the laminar burning velocity, S_L, at the corresponding pressure, similar to the diffusive limit found in the earlier hydrogen/air DNS study [16]. From the simulations, S_L of T_0 = 850, 934, and 1008 K are found to be approximately 0.2, 0.25, and 0.32 m/s, respectively. Note that these speeds do not change much with variations in the strength of the ignition source and the variation of the laminar flame speed with pressure is also less than 10 % of mean values. Therefore, henceforth the laminar flame speeds described above provide a reference for comparison with S_d^*.

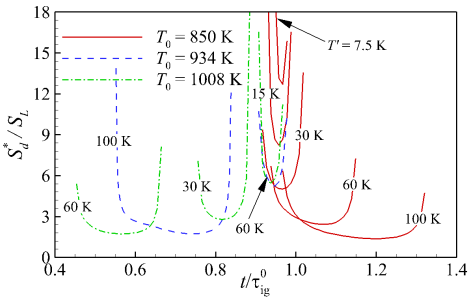

Figure 7. Temporal evolution of the front speed, S_d^*, of 1-D reference cases with different T_0 and T'

Figure 7 shows the temporal evolution of the front speed, S_d^*, for the 1-D DNS cases with different T_0 and T' corresponding to all of the two-dimensional DNS cases. Nominally, the curves exhibit a characteristics 'U' shape, also observed in previous studies [16, 17]. Consistent with the two-dimensional DNS cases, overall combustion is advanced with increasing T' for cases with T_0 = 934 and 1008 K, but retarded for cases with T_0 = 850 K. Note also that, for all cases, during incipient thermal runaway, S_d^* of the nascent ignition kernel is significantly larger than the laminar flame speed, S_L. S_d^* is unbounded in

the nascent ignition kernel since the scalar gradient, $|\nabla Y_k|$, in Eq. (1) vanishes [17, 35]. Similarly, burnout of the remaining charge results in an abrupt thermal runaway due to compression heating, and thus, S_d^* is also unbounded there as shown in Fig. 7. Between the two singularities in S_d^*, however, deflagration of relatively constant speed is predominant for cases with large T', and hence, S_d^* exhibits values close to S_L with increasing T'.

Figure 7 also shows that the duration of the region of constant speed at the bottom of the 'U' shape increases with increasing T', suggesting that combustion at the reaction waves occurs primarily by deflagration rather than by spontaneous ignition. On the contrary, for cases with small T', the front speed is much greater than S_L to the extent that, for some cases, it is too large to be shown in Fig. 7 (e.g., T_0 = 934 K and T' = 15 K). Therefore, a small degree of thermal stratification leads an excessive rate of heat release due to simultaneous auto-ignition occurring throughout the whole domain, which should be avoided in HCCI combustion. These results also suggest that the critical degree of thermal stratification for smooth operation of HCCI engines depends on the mean initial temperature T_0, and hence, both initial T_0 and T' need to be considered to curtail too large a pressure rise rate.

The temporal evolutions of the mean front speed, $\overline{S_d^*}$, for the two-dimensional DNS cases is presented in Fig. 8. Note that the mean front speeds also exhibit a characteristic 'U' shape qualitatively similar to the corresponding one-dimensional cases. Comparison between Figs. 5 and 8 verifies that deflagration waves develop past initial thermal runaway for the cases with large T' as in the one-dimensional cases. Moreover, deflagration waves appear earlier and persist longer than the corresponding one-dimensional cases, simply because the large T' results in locally hotter mixtures than are present in the one-dimensional cases, and hence, locally auto-ignition can occur and evolve into a deflagration wave sooner than in the one-dimensional cases.

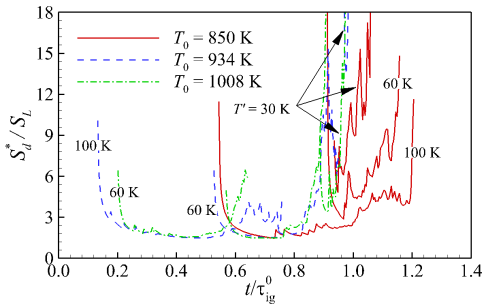

Figure 8. Temporal evolution of the front speed, $\overline{S_d^*}$, of 2-D DNS cases with different T_0 and T'

A quantitative measure of the occurrence of deflagration and spontaneous ignition modes in the combustion process is obtained from the temporal evolution of the fraction of heat release rate occurring in the deflagration mode as shown in Fig. 9. To distinguish between the two modes of propagation, the Damköhler number, Da, defined by [34], is adopted:

$$Da = \frac{\dot{\omega}_k}{|-\partial(\rho Y_k V_{j,k})/\partial x_j|}, \qquad (2)$$

where Y_c is used to evaluate Da. From 1-D simulations, it is found that Da in the diffusive limit is approximately 4.0. The departure from unity is because, although the combustion wave propagates under the diffusive limit, the upstream mixture is highly reactive and hence, the reaction term is somewhat larger than the diffusion term. In the present study, the delineation between the two propagation modes is defined by Da less than 4.0 (deflagration wave).

Several observations can be made from Fig. 9. First, at the initial and final stages of the ignition, the fraction of $\overline{\dot{q}}$ from the deflagration mode becomes unity simply because the corresponding reaction rate vanishes, and thus, Da also vanishes. Second, the fraction of $\overline{\dot{q}}$ from the deflagration mode increases with increasing T', such that over half of the heat release rate occurs in the deflagration mode between the first- and the second-stage ignition for cases with large T'. Third, for small T', the fraction of $\overline{\dot{q}}$ from the

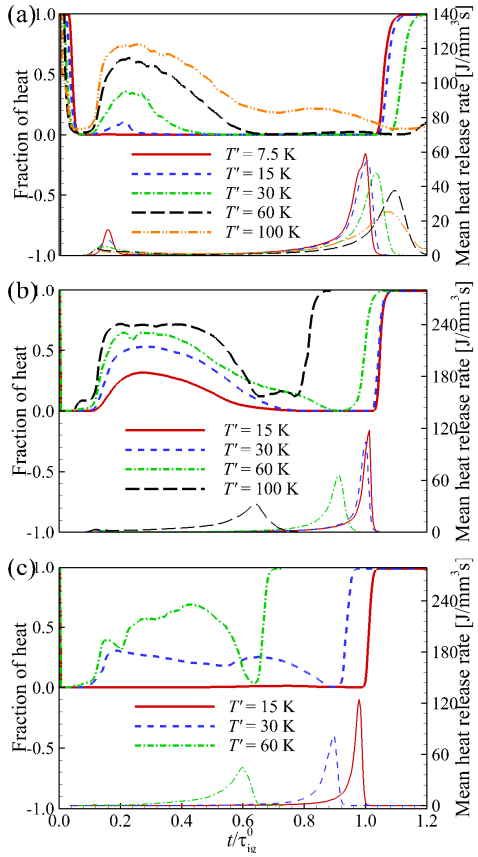

Figure 9. Temporal evolution of fraction of heat release rate from the deflagration mode (thick lines) and heat release rate (thin lines) with different temperature RMS: (a) T_0 = 850, (b) 934, and (c) 1008 K.

deflagration mode vanishes much sooner than the occurrence of the peak $\bar{\dot{q}}$; on the contrary, for large T' (i.e., Cases 5, 9, and 12), a considerable fraction of $\dot{q}$ still occurs in the deflagration mode at the point when $\bar{\dot{q}}$ peaks. As discussed earlier in reference to the one-dimensional DNS cases, at the final stage of ignition, the remaining unburned charge is heated by compression and consumed as simultaneous ignition, exhibiting large values of S_d^*. Therefore, only a small fraction of combustion occurs in the deflagration mode during the final stages of ignition, verifying that spontaneous auto-ignition occurs for small T'. However, a relatively large fraction of the deflagration mode with large T' indicates the occurrence of mixed modes of deflagration and spontaneous ignition. These results, further, verify that deflagration is attributed to spreading out the heat release rate.

4. Conclusion

The effects of thermal stratification (through both mean and fluctuations in initial temperature) and turbulent mixing timescales on auto-ignition of a lean homogeneous *n*-heptane/air mixture at constant volume and high pressure are investigated by direct numerical simulations with a new 58-species reduced *n*-heptane/air kinetic mechanism. In the first parametric study, the homogeneous ignition delay was held constant, and twelve cases with varying initial mean temperature straddling the NTC regime were studied with different degrees of temperature fluctuations imposed. The displacement speed, Damköhler number, and chemical explosive mode analyses verify that, in general, larger T' induces greater spreading of the mean heat release rate because the deflagration mode is predominant at the reaction fronts for large T'. However, spontaneous ignition prevails for small T', and hence, simultaneous auto-ignition occurs throughout the whole domain, resulting in an excessive rate of pressure rise. For mean temperatures lower than the NTC region, e.g. with T_0 = 850 K, the ignition delay is retarded with increasing T'. On the contrary, the ignition delay is significantly decreased with T' for mean temperatures greater than the NTC region (e.g. T_0 = 1008 K). For mean temperatures within the NTC region, e.g. with T_0 = 934 K, the combined effects of high and low temperature manifest themselves such that the ignition delay is retarded for small T' but is advanced with large T'.

These results imply that the critical degree of thermal stratification for smooth operation of HCCI engines depends on both the mean initial temperature and the level of fluctuations. Therefore, both mean and fluctuations of initial temperature should be considered to control ignition timing of HCCI combustion and to alleviate the excessive rate of pressure rise.

Acknowledgement

This conference paper is a part of a paper submitted to Combustion and Flame (2010). The work at Ulsan National Institute of Science and Technology (UNIST) was supported by the 2009 Research Fund of UNIST. The work at University of Connecticut was supported by the National Science Foundation under Grant No. 0904771. Any opinions, findings, and conclusions or recommendations expressed in this material are those of the authors and do not necessarily reflect the views of the National Science Foundation. The work at Sandia National Laboratories (SNL) was supported by the Division of Chemical Sciences, Geosciences, and Biosciences, Office of Basic Energy Sciences, and Office of Advanced Scientific Computing Research of the US Department of Energy. JHC was also supported as part of the Combustion Energy Frontier Research Center, an Energy Frontier Research Center funded by the U.S. Department of Energy, Office of Science, Office of Basic Energy Sciences under Award Number DE-SC0001198. SNL is a multiprogram laboratory operated by Sandia Corporation, a Lockheed Martin Company, for the US Department of Energy under contract DE-AC04-94AL85000.

References

[1] J. E. Dec, Proc. Combust. Inst. 32 (2009) 2727-2742.
[2] M. Yao, Z. Zheng, H. Liu, Prog. Energy Combust. Sci. 35 (2009) 398-437.
[3] J. E. Dec, W. Hwang, M. Sj"Noberg, SAE Trans. (2006) 2006-01-1518.
[4] J. A. Eng, SAE paper (2002) 2002-01 - 2859.
[5] A. Hultqvist, M. Christenson, B. Johansson, M. Richter, J. Nygren, J. Hult, M. Alden, SAE paper (2002) 2002-01-0424.
[6] A. Babajimopoulos, G. A. Lavoie, D. N. Assanis, SAE paper (2003) 2003-01-3220.
[7] J. E. Dec, W. Hwang, SAE Trans. paper (2009) 2009-01-0650.
[8] M. Sjöberg, J. E.Dec, SAE Trans. paper 115 (2006) 318-334.
[9] W. Hwang, J. E. Dec, M. Sj"Noberg, SAE Trans. paper 116 (2007) 2007-01-4130.
[10] J. E. Dec, M. Sjöberg, SAE Trans. paper 112 (2003) 2003-01-0752.
[11] R. R. Steeper, S. D. Zilwa, SAE paper (2007) 2007 - .01 - .0180.
[12] P. W. Aroonsrosopon, P. Werner, J. O. Waldman, SAE Tran. paper 113 (2004) 2004-01-1756.
[13] J. Hyvönen, G. Haraldsson, B. Johansson, SAE paper (2005) 2005-01-0109.
[14] H. Persson, A. Hultqvist, B. Johanass, A. Remón, SAE paper (2007) 2007-01-0212.
[15] R. Sankaran, H. G. Im, E. R. Hawkes, J. H. Chen, Proc. Combust. Inst. 30 (2005) 875-882.
[16] J. H. Chen, E. R. Hawkes, R. Sankaran, S. D. Mason, H. G. Im, Combust. Flame 145 (2006) 128-144.
[17] E. R. Hawkes, R. Sankaran, P. P"Lebay, J. H. Chen, Combust. Flame 145 (2006) 145-159.
[18] Y. B. Zeldovich, Combust. Flame 39 (1980) 211-214.
[19] S. Liu, J. C. Hewson, J. H. Chen, H. Pitsch, Combust. Flame 137 (2004) 320--339.
[20] S. Liu, J. C. Hewson, J. H. Chen, Combust. Flame 145 (2006) 730-739.
[21] G. Bansal, H. G. Im, S. R. Lee, Proc. Combust. Inst. 32 (2009) 1083-1090.
[22] H. G. Im, J. H. Chen, C. K. Law, Proc. Combust. Inst. 27 (1998) 1047-1056.
[23] T. Echekki, J. H. Chen, Combust. Flame 134 (2003) 169-191.
[24] S. Tanaka, F. Ayala, J. C. Keck, J. B. Heywood, Combust. Flame 132 (2003) 219-239.
[25] X. Lü, L. Ji, L. Zu, Y. Hou, C. Huang, Z. Huang, Combust. Flame 1449 (2007) 261-270.
[26] A. Dubreuil, F. Foucher, C. Mouaï.m-Rousselle, G. Dayma, P. Dagaut, Proc. Combust. Inst. 31 (2007) 2897-2886.
[27] G. B. Jr., J.-Y. Chen, R. W. Dibble, Proc. Combust. Inst. 32 (2009) 2877-2884.
[28] D. A. Rothamer, J. A. Snyder, R. K. Hanson, R. R. Steeper, R. P. Fitzgerald, Proc. Combust. Inst. 32 (2009) 2869-2876.
[29] J. H. Chen et al., Comput. Sci. Disc. 2 (2009) 015001.
[30] C. A. Kennedy, M. H. Carpenter, Appl. Num. Math. 14 (1994) 397-433.

[31] C. A. Kennedy, M. H. Carpenter, R. M. Lewis, Appl. Num. Math. 35 (2000) 117-219.

[32] R. J. Kee, F. M. Rupley, E. Meeks, J. A. Miller, CHEMKIN-III: A fortran chemical kinetic package for the anaylsis of gas-phase chemical and plasma knietics, Tech. Rep. SAND96-8216, Sandia National Laboratories (1996).

[33] R. J. Kee, G. Dixon-Lewis, J. Warnatz, M. E. Coltrin, J. A. Miller, A fortran computer code package for the evaluation of gas-phase multicomponent transport properties, Tech. Rep. SAND86-8246, Sandia National Laboratories (1986).

[34] R. J. Kee, J. F. Grcar, M. D. Smooke, J. A. Miller, A fortran program for modeling steady laminar one-dimensional flames, Tech. Rep. SAND85-8240, Sandia National Laboratories (1985).

[35] C. S. Yoo, R. Sankaran, J. H. Chen, J. Fluid Mech. 460 (2009) 453-481.